Effect of wall light reflection in ITER diagnostics

Shin Kajita
IMaSS, Nagoya University, Nagoya 464-8603, Japan
E-mail: kajita.shin@nagoya-u.jp

Marie-Helene Aumeunier
CEA, IRFM, F-13108 Saint-Paul-Lez-Durance, France

Eiichi Yatsuka
QST, Ibaraki 801-1, Japan

Andrey Alekseev, Evgeny Andreenko
NRC Kurchatov Institute, Kurchatov sq. 1, 123182 Moscow, Russia

Alexander Kukushkin
NRC Kurchatov Institute, Kurchatov sq. 1, 123182 Moscow, Russia
NRNU MEPhI, Kashirskoye sh. 31, 115409 Moscow, Russia

Vladislav Neverov
NRC Kurchatov Institute, Kurchatov sq. 1, 123182 Moscow, Russia

Martin Kocan, Michele Bassan, Evgeny Veshchev, Maarten De Bock, Robin Barnsley
ITER Organization, 13067 St. Paul Lez Durance Cedex, France

Andrei Kukushkin
NRC Kurchatov Institute, Kurchatov sq. 1, 123182 Moscow, Russia
NRNU MEPhI, Kashirskoye sh. 31, 115409 Moscow, Russia

Roger Reichle, Michael Walsh
ITER Organization, 13067 St. Paul Lez Durance Cedex, France

Abstract. Reflection of light on walls will result in parasitic signals for various optical diagnostics and can be a serious issue in ITER. In this study, we show recent progress in the assessment of the effects of the wall reflections in ITER based on ray tracing simulation results. Four different diagnostics in ITER were chosen for the simulation, i.e., visible spectroscopy, infrared thermography, edge laser Thomson scattering, and charge exchange recombination spectroscopy.

1. Introduction

Electromagnetic waves in a wide wavelength range are used for various purposes in nuclear fusion devices, especially for plasma diagnostics. It has been identified on various fusion devices that the reflection of electromagnetic waves inside the vacuum vessel can disturb measurement results. In the DIII-D tokamak, where graphite wall tiles were used, it was shown that D_α and CIII emission can be perturbed by a factor 2 or more by reflection of light coming from the divertor in some main chamber view chords [1, 2]. Moreover, in recent ITER-like wall (ILW) experiments at JET, an order of magnitude greater stray light was identified in H_α diagnostics [3]. In the Tore Supra tokamak, it was reported that Z_{eff} measurement was systematically overestimated for the edge channels due to reflection [4]. To deal with the reflection issue on Z_{eff} in the ASDEX Upgrade tokamak [5], a special data analysis method called Integrated Data Analysis in the framework of Bayesian probability theory has been utilized [6, 7]. Moreover, the influence of reflection on infrared (IR) imaging in Tore Supra [8] and in the JET-ILW [9] has been investigated.

In ITER, the inner wall will consist of tungsten (W) for the divertor and beryllium (Be) for the main chamber, which have higher optical reflectivity than carbon based materials, and, moreover, the contrast in the plasma emission profile between the brightest part and dark regions could be greater than in present devices. Thus, there is a concern that the effects of the reflection of electromagnetic waves would be more significant than those in the present devices and have a great impact on the ITER operation. For example, background light reflection on the first wall would degrade signal to noise ratio of laser aided spectroscopy and active spectroscopy. Misinterpretation of the IR measurement could strongly hamper the ITER operations and the scenario development by excessive interruptions of the plasma shots or, on the contrary, by endangering the machine safety in the case of underestimation of the surface temperature. It is of importance to investigate the influence of reflections for all diagnostics relying on light emissions and deal with them properly before starting the ITER operation.

The modelling of reflection in ITER has been conducted for passive spectroscopy [11, 12, 13], active spectroscopy [14, 15], and infrared thermography [16, 10]. Concerning visible spectroscopy, the effect of reflection of H_α and beryllium (Be) emission in ITER on scrape off layer (SOL) view chords [11] and divertor view chords [12] has been investigated. It was found that the stray light level in the SOL field of view can be orders of magnitudes higher than the signal of interest (i.e. the line emission from the SOL) due to reflection of the emission from the divertor region. For IR imaging, in addition to the assessment of reflection [16], optical blur due to finite IR detector size was revealed [10].

In this study, we show the recent progress of the modelling of photon reflection based on ray tracing simulations with brief review of current status and discuss the influence quantitatively. For visible spectroscopy, simulations are conducted using LightTools

[18] and Zemax [19], and practical method for mitigation of stray light are discussed. For IR measurement, a Monte Carlo ray tracing code (SPEOS ® CAA V5 [20]) was used to assess the impact of changing radiative properties of materials (emissivity and reflectivity) on the surface temperature measurement. Moreover, the influence of the reflection of emission from divertor on edge laser Thomson scattering diagnostics and the influence of the reflection of strong edge signal on charge exchange recombination spectroscopy (CXRS) are shown.

2. Visible passive spectroscopy

2.1. Stray light level assessment

In the following simulations, a computer-aided design (CAD) model of a 20° toroidal sector of the ITER vacuum vessel including first wall and divertor was imported in the LightTools model. Boundary conditions to this 20° toroidal sector were implemented by two perfect mirrors. This configuration is valid if the emission source is toroidally uniform. The detailed optical system was approximated by a two-dimensional pinhole camera. The emission profiles calculated by the SOLPS4.3 code (B2-Eirene) and DIVIMP [21] were imported into the LightTools model. Backward ray tracing method, in which rays were traced from the receiver through the pinhole, was used for the simulation.

Figures 1(a) and (b) present the irradiance profiles of H_α without and with wall reflection, respectively, in a low density L-mode discharge scenario (case d in [11]). In Fig. 1(b), the reflectivity was assumed to be 50% divided over 25% Lambertian reflectivity and 25% specular reflectivity (with a Gaussian profile of 6° in half-width). The field of view corresponds to the one from the receiver B in Fig. 2. From the investigation of the dependence on the reflection property, it was found that the stray light level is not very sensitive to the ratio of specular to diffuse reflection, especially when the emission source is toroidally uniform [11]. However, in some specific situations, e.g. when the source in not toroidally uniform, the stray light level can be very sensitive to this ratio; one such case will be shown in Sec. 5. Note that considering full ray tracing to obtain the 2 dimensional profile with reflection requires significant computational performance. The calculation time was significantly shortened, due to the improvement in the performance by parallel processing via multi-CPU/core machines, when moving to the LightTools 8.1. release. It is seen that the emission from the divertor region is so strong that the divertor stray light (DSL) dominates the irradiance profile when considering the wall reflections. Typically the stray light was two orders of magnitude greater than the SOL signal intensity.

In Fig. 1(b), the profile was almost flat and significant non-uniformity was not identified in logarithmic scale. However, when increasing the spatial resolution of simulation, it was identified that the stray light level can be altered by the shape of the wall and viewing angle. We investigated the detailed stray light profile at a higher

resolution with two different viewing angles from receivers A and B, as shown in Fig. 2(a). Figures 2(b) and (c) show 2 dimensional irradiance profiles at the upper and lower receivers, respectively. In this calculation, the total reflectivity was assumed to be 50% with 25% diffuse and 25% specular reflectivity. In Figs. 2(b) and (c), the blanket modules (BMs) can be identified in the irradiance profile. The BMs 1-7 can be seen on the upper receiver, and the BMs 1-6 and a part of divertor cassette can be seen on the lower receiver. In both cases, a bright area exists around BM 5, and a bright line was identified at the bottom part of BM 2. It is identified that the brightness around BM 5 is approximately twice higher on the upper receiver compared with the lower receiver. Also, the bright line on BM 2 is brighter at the upper receiver. The variations in the bright spots could be due to the difference of the specular reflection components from the divertor.

In addition to the LightTools, we started to use the "Zemax OpticStudio" software package to assess the effects of optical dump in particular. One of the major reasons to use Zemax is its better usability. The license of Zemax is cheaper than that of LightTools, and, also, Zemax has been widely used to design optics. If it was verified that Zemax can also be used for stray light assessment, various detailed assessments can be done. One of the major reasons is in the fact that license of LightTools is much more expensive than that of Zemax. And, also, there are many people who can use Zemax to design optics. If it was verified that Zemax can also be used for stray light assessment and various detailed assessments can be done. Before using the Zemax software, we conducted a comparison between LightTools and Zemax to verify the results of both models against each other, using the same configuration and sources as used in Fig. 1. For this benchmark, a simplified model with a smoothed ITER first wall was used to ease the Zemax code operation, while all other parameters were the same as those in [11]. The ratio of specular to diffuse reflectivity was assumed to be 1/49 in this calculation with the reflectivity of 50%. Backward ray tracing was used in LightTools, while forward ray tracing was used in Zemax. In Fig. 3, comparisons of the radiance profiles calculated by the LightTools and Zemax, respectively, are shown with and without reflection. Although the noise level is slightly higher in Zemax, probably because of low statistics in the number of rays due to forward ray tracing in Zemax, the radiance profiles agree well with each other in both with and without reflection. The Zemax simulation will be used in the later calculation for optical dumps.

2.2. Design of optical dumps

For the necessary reduction of the stray light level, various methods can be used. For the divertor impurity monitor, where the stray light level is typically comparable to or less than the signal, it was confirmed that ray tracing can somewhat mitigate the stray light by reconstructing the original emission profile with considering the modelled reflections on walls [22]. For spectroscopy in the SOL region, where the stray light can be orders of magnitude greater than the actual signal, it was assessed [11] that optical

dumps could reduce the stray light level by an order of magnitude. Moreover, the special measurement scheme proposed in [23], which uses optical dumps along with the line of sight (LoS) targeted at the neighboring area of the first wall (so called bifurcated LoS scheme), can allow to subtract the unknown spectral contribution of the DSL from the total signal. Using Zemax simulations of the DSL spectral intensity, the efficiency of optical dumps was investigated with different reflection properties of the optical dumps for various design and locations [24] using the principles of the Hα synthetic diagnostic [13].

This synthetic diagnostic estimates the errors of the solution of the inverse problems aimed at recovering the neutral hydrogen parameters in the SOL from the high resolution spectrum shape with allowance for (i) strong DSL on the observation chords in the main chamber, (ii) substantial deviation in the velocity distribution function of neutral atoms from a Maxwellian in the SOL, and (iii) the data from the direct observation of the divertor. The results of recovering the relative contributions of all three sources to the signal along a LoS in the main chamber, namely, the emissions from the plasma at different magnetic field strengths (e.g., on the LFS and HFS sections on the LoS) and the DSL, together with the isotope ratios in the SOL, were presented for the flat-top stage of $Q = 10$ inductive operation of ITER. The error assessment for the LoS along the major radius from the equatorial port-plug in ITER in [13] showed that (i) without the DSL, the absolute value of the error of estimating the fraction of the HFS SOL light in the total signal does not exceed 0.2; (ii) already for a 40% fraction of the DSL in the total signal, the absolute error of recovering the contributions of the HFS and LFS SOL emission is unacceptably high, say 0.4, because of the poor accuracy of predicting the DSL; (iii) recovery of the isotope ratio of the tritium-deuterium mixture, that is more complicated than for the hydrogen-deuterium mixture, is not feasible with a sufficient accuracy even without the DSL. Further extension of the approach is, therefore, needed.

An application of this approach to exploit high-resolution spectroscopy data, without using optical dumps, using recent JET-ILW experiments enabled [25] to evaluate the spectrum of the DSL and the signal-to-background ratio for Balmer-alpha light emitted from the far SOL and divertor in JET-ILW. High-resolution spectroscopy data, with a resolving power sufficient to distinguish the deuterium and hydrogen spectral lines of Balmer-alpha series, were analysed for a direct observation of the divertor from the top and for an observation of the inner wall along tangential and radial LoS from equatorial ports. The results showed the importance of non-Maxwellian effects (and respective asymmetry of the spectral line shape) in the interpretation of the Balmer-alpha high-resolution spectroscopy data, especially on the radial LoS, where the strong inward flux of fast atoms from the wall substantially distorts the conventional Gaussian spectral line shape of the local emissivity and, consequently, the observed intensity on the LoS. On the whole, the results support the expectation of a strong impact of the DSL upon the ITER main chamber Hα (and visible light) spectroscopy diagnostics and the necessity of using the optical dumps in ITER.

The measurement scheme [23] is effective only if the optical dump, which suppresses

the DSL, does not distort its normalized spectral shape. Figure 4 shows the simulated DSL spectrum reflected from the first wall to the ITER equatorial port-plug with the ZEMAX code for various types of optical dumps on BM 4: a simple cylinder, a bolt hole, a cylinder with a conical bottom and a cylinder with diaphragms. It is identified that cylindrical shaped optical dumps reduce the DSL up to an order of magnitude. Moreover, additional diaphragms can decrease the DSL further, typically, to 1/50. From the comparison in the spectrum shape in a detailed manner, it was found that optical dump may also slightly distort the DSL spectrum, up to ∼10%, and decreases the accuracy of spectrum analysis [24]. It would be necessary to take into consideration the error caused by the distortion of spectrum when analysing the detailed shape of the spectrum.

3. Infrared thermography

Infrared thermography is a key diagnostics for the machine protection, in particular for monitoring of the surface temperature of the plasma facing components, $T_{\rm surf}$. Nevertheless, wall light reflections and low and variable emissivity are very damaging for infrared measurement interpretation. This can hamper the experimental programs by triggering a fast termination of plasma, whilst the real hot spots might not be detected.

In order to anticipate the IR measurements in such a metallic environment, a photonic simulation was performed using a Monte Carlo ray tracing based on SPEOS ® CAA V5 able to propagate the light in a 3-D complex environment and integrating the photon-material interaction. Such a simulation must provide "realistic" synthetic data such as that obtained with the real instrument. The accurate prediction of the measurements will depend on the capability of modelling accurately all physical processes involved in the measurements, i.e.: (1) the plasma heat loads deposit and the resulting surface temperature of in-vessel components for different plasma scenario, (2) the radiative properties of materials (reflectivity and emission models), and (3) the infrared wide-angle imaging system.

Figures 5(a) and (b) show synthetic infrared images of the ITER Wide Angle Viewing System (WAVS) of equatorial port plug (#17) and for the left tangential view without reflection (actual temperature profile) and with reflection, respectively. In those simulations, a baseline burning plasma equilibrium has been considered. The surface heat loads have been computed with the plasma current $I_p = 15$ MA, edge safety factor $q_{95} = 3$ and the distance between the primary and the secondary separatrix $\Delta_{sep} = 9$ cm at the outboard midplane [17]. The surface emission is modelled using the n-cosines power model as a function of viewing angle with $n = 0.6$ and by considering uniform emissivity independent of the wavelength, of 0.2 and 0.15 respectively for W and Be materials. The assumption of the n-cosine model is roughly consistent with experimental data in [26]. The reflectivity on the metallic surfaces is modelled as a combination of Lambertian and specular components. The study aimed to evaluate the impact of reflections by considering extreme values of surface roughness: a diffuse

model (100% Lambertian) and a highly specular model (2% Lambertian) following a Gaussian shape with a full-width half maximum of 12° [27]. The optical model aimed to reproduce the camera view by taking into account the camera geometrical parameters (field-of-view, image size in the focal plane, and wavelength range) without including the possible optical effects on resolution (diffraction and pixel cross-talk).

Such a simulation allows evaluating the part of reflected flux ("parasitic light") within the total flux collected by the camera and identifying the main contributor causing reflection features. It was estimated from the results in Fig. 5(a,b) that the contribution of reflections in the IR image is larger than 75%. The contribution of reflected flux is slightly higher in a case of a diffuse surface (>85%). However, materials with specular surfaces cause remarkable light patterns in the infrared images which may be confused with enhanced, potentially dangerous, localized heat flux. Concerning the surface temperature measurements from infrared images, the measurement error due to reflections depends also on the precise knowledge of the emissivity value, ϵ. In Fig. 5(b), the emissivity was assumed to be known (gray body). Because the actual emissivity value can alter during the operation and can be difficult to verify, blackbody is often assumed with $\epsilon = 1$. This leads, however, to underestimation of the temperature in the hot regions, as shown in Fig. 5(c). The temperature was underestimated up to 40% in the hot region on outer vertical target. For intermediate temperatures in the range of 175-200°C, emissivity and reflection compensate each other and T_{surf} was estimated within 20% of accuracy. Figure 6 shows predicted gray body temperature profiles on the inner vertical targets in the case of diffuse and specular materials. By correcting only emissivity, the surface temperature of colder target is always overestimated by 50-100% due to the reflections. This especially impacts on the decay length measurement from the peak target profile in the diffuse case. The diffuse case is more unfavorable with an error of 40% on the decay length, but the fit in the specular case is more difficult due to the non-uniformity of the reflections contribution along the peak profile. The treatment of emissivity and reflections to deduce the true surface temperature by resolving inverse problem using the direct photonic simulation is currently underway.

Such a synthetic diagnostic provides an indispensable tool for helping the infrared image interpretation and getting more confidence in the surface temperature measurement in ITER. Now, the next challenge is to strengthen the confidence in the method by consolidating the different physical models involved in this end-to-end simulation from the model of the thermal environment to the radiative properties of in-vessel components and the instrumental model. To do that, WEST [28] upgrade and ASDEX-Upgrade will be used as the benchmark to compare and adjust simulated infrared images with experimental data. In parallel, laboratory experiments will be performed to characterize the materials features (emissivity and reflectivity) and this as a function of surface roughness to take into account the possible change during the machine life.

4. Laser Thomson scattering

The major noise source for laser Thomson scattering is background photon noise. It is possible to reduce the photon noise by shortening the pulse width (time duration) of the laser beams. However, laser-induced damage on the beam dump is concerned when the pulse duration is extremely short, because the damage threshold is sensitive to the peak power rather than to the energy.

Although only bremsstrahlung radiation from the core should be taken into account when the reflection is not significant, it is necessary to assess the impact of the reflected line radiation from the divertor region in ITER. The diagnostic laser beam has the wavelength of 1064 nm. The scattered light spectra can be broader than the range from ∼500 to 1500 nm when the electron temperature is 10 keV. The edge Thomson scattering uses scattered light with a wavelength less than 1064 nm. Figure 7 shows a comparison of calculated radiation power between the bremsstrahlung and line emissions from the divertor and SOL regions. Profiles of emissivity were calculated based on SOLPS4.3 modelling for the carbon-free ITER divertor case with Ne seeding, and the radiation power was summed up for the whole region modelled. In the calculation, it was assumed that the peak thermal flux on the divertor target was 10 MW/m^2 and total radiated power was 43 MW. The bremsstrahlung is integrated over 100 nm intervals for wavelengths above 600 nm and over 150 nm below. It can be seen that there are several strong emission lines of beryllium and helium in addition to those of deuterium. Eight lines were above the level of the bremsstrahlung, and it would be better to eliminate them by filters in the spectrometers for Thomson scattering systems in ITER if the reflection of those lines is significant.

Ray-tracing simulations on the level of background light were carried out to assess the performance and availability of the Thomson scattering diagnostics. In the edge Thomson scattering system of ITER, there is an intermediate image of the laser beam between the fourth and fifth mirrors (M4 and M5) [29]. As shown in Fig. 8, the collection optics of edge Thomson scattering system was modelled precisely up to M4 in LightTools and intensity of the background light was evaluated along the intermediate image. There is one-to-one relationship between the positions on the laser beam and the intermediate image. The aperture of the first wall was also modelled precisely to restrict the direction of light coming from the plasma side.

Figures 9(a-c) show the expected intensities of background light on each line of sight in the wavelength ranges of 450-600, 700-800, and 900-1000 nm, respectively. The solid and the dotted lines correspond to the cases with and without reflection, respectively, and the bremsstrahlung from the core and from the edge and the line emission was plotted separately with different colors. The total amount of bremsstrahlung from the core plasma increases typically by ∼50% by the reflection. Compared with the bremsstrahlung from the core, that from the divertor and SOL has less influence even though the density is higher and temperature is lower in the divertor region. This is because the total radiation volume in the region is much smaller than that of the core.

On the other hand, line emissions coming from divertor plasma increased significantly by the reflections on the first wall in 450-600 and 700-800 nm wavelength ranges and exceeded the bremsstrahlung radiation from the core. The accuracy of the Thomson scattering measurement was evaluated in the same manner as in [29] by considering the influence of the wall reflection. Although the detailed assessment will be reported elsewhere, it was confirmed that the measurement can be conducted with the required accuracies in the electron temperature (<10%) and density measurements (<5%) even considering the reflection by using a laser with the laser pulse energy and the pulse width of approximately 4 J and 4 ns, respectively. Optimization of the laser pulse energy and pulse width for various discharge scenarios is of interest for our future work by considering the effect of reflection and damage of laser beam dump.

5. CXRS

In active spectroscopy, like CXRS, wall reflections can lead to various sources of error. Three error sources associated with reflection were considered in [15] where ray tracing simulations were performed with LightTools: (i) influence of strong CXRS emission from the plasma edge (where the neutral beam is hardly attenuated) reflected into the CXRS viewing chords of the plasma core (where the local CXRS emission of interest is very weak due to strong neutral beam attenuation), (ii) disturbance of the CXRS spectrum by the line emission from the divertor region (cold component) and (iii) increase in the noise by the reflected continuum (bremsstrahlung) radiation.

Points (ii) and (iii) are similar to the effects found in the relections assessment of the Thomson scattering diagnostics. It was found that the reflected line emission from the divertor (cold component) can be significantly greater than the CXRS signal of interest. In the worst case, where the broad CXRS He II emission line (468.5nm) from the plasma core (>10 keV) overlaps with the same but narrow He II emission line reflected from the divertor (<10 eV), the peak height of the reflected He II divertor emission can be more than five orders of magnitude higher than the peak of the core He II CXRS emission line. Although the CXRS line can be distinguished from the reflected divertor emission line thanks to their difference in line width, the strong variation in peak height could lead to saturation of the detector. This indicates that special care would be necessary when designing the spectrometer and choosing the detector (e.g. ensuring sufficient dynamic range and/or masking of the strong divertor emission line). With respect to point (ii), it was found that the background bremsstrahlung could be double by the reflection, increasing the noise level.

Concerning the above item (i), i.e. the influence of the reflected edge CXRS emission (coming from where the neutral beam enters the plasma) onto the core CXRS measurement, it was found that the stray light level is sensitive to the ratio of diffuse to specular reflection. It was found that the signal from the edge can be harmful near the core region especially when the diffuse reflectivity component is significant. Figure 10 shows the stray light level profiles in a high density scenario for different diffuse over

specular reflection ratios. For this calculation, a full 3-dimensional (360° toroidally) model of the ITER wall was constructed in LightTools and used, because the CXRS signal is, in contrast to the passive spectroscopy cases, not toroidally uniform. The stray light level was calculated by subtracting the intensity without reflection from the one with reflection. Two cases are shown with the ratio of diffuse to specular reflectivity, $R_{\rm d}/R_{\rm s}$, 25/25 and 1/49, respectively. In both cases, the stray light level is higher in the core. This is because the CXRS signal decreases from the edge to the core; in the high density scenario, the intensity decreases by three orders of magnitude due to the attenuation of the beam intensity. The scatter in the data of figure 10 is solely due to the reflections; as was shown previously in [15], the intensity profile without stray light does not have scatter. Comparing the two cases, it is seen that the stray light level has more scattering in specular case, i.e. when $R_{\rm d}/R_{\rm s}$=1/49, compared to the diffusive case. With increasing the diffuse reflectivity, the stray light profile became flatter, similar to the case of passive spectroscopy [11]. However, also the stray light level significantly altered when we changed $R_{\rm d}/R_{\rm s}$; if the diffuse component is higher, the stray light level becomes higher.

Figure 11(a) and (b) shows the ratio of the stray light to the signal at ρ =0.0, 0.3, 0.5, 0.9 in low density and high density scenarios, respectively, as a function of the ratio $R_{\rm d}/R_{\rm s}$. The scattering of the stray light profile is represented with error bars. Typically, the scattering is 20-30% when the diffuse reflection component is dominant, and it increases to greater than 100% with decreasing the diffuse reflection fraction. It is seen that the stray light level is significantly decreased in the range $0< R_{\rm d}/R_{\rm s} < 20$ %. When $R_{\rm d}/R_{\rm s} \sim 20\%$, the stray light can be ∼20% in the core. The results suggested that the reflected CXRS signal can be an issue especially in high density cases, though it strongly depends on the diffuse reflection fraction. Because the CXRS diagnostics cover the full plasma region and because the main contribution to the stray light is from the edge CXRS emission, it may be possible to extract the stray light components by analyzing the CXRS spectrum of the outer viewing chord (most near the edge) first, assuming negligible stray light, and use the analysed properties (intensity and line width) as input for the stray light component of the next, more inward chord. For next chord the stray light component can be estimated from the analysis of the previous 2 chords et cetera, working towards the chords in the plasma core in an iterative way. Further studies about the methodology to eliminate the stray light would be of interest for future work. Also, the result suggested that the bidirectional reflectance distribution function (BRDF) is important to know to assess the influence of the reflected stray light on the active CXRS signal; similar to the case of the IR stray light.

6. Conclusions

The reflection of visible and infrared radiation was investigated using ray tracing simulations and the effects on Hα spectroscopy, infrared thermography, edge laser Thomson scattering, and CXRS were discussed based on the simulation results. For

Hα spectroscopy of the scrape off layer region, it was shown that the stray light could be much greater than the actual signal level, indicating that the stray light from the divertor could be a serious issue. It was shown that an optical dump can mitigate the divertor stray light up to two orders of magnitude by adding a diaphragm on a cylindrical optical dump. However, optical dumps can slightly change the shape of the Hα spectra, typically 10%, suggesting the necessity of taking this slight distortion into account when performing a detailed analysis. For infrared thermography, in addition to the influence of reflection, there is a difficulty due to the unknown emissivity, ϵ, to obtain the temperature profile from the IR camera image. If blackbody is assumed with $\epsilon = 1$, the temperature in hot regions, typically higher than 275°C, is underestimated. In colder regions, the temperature could be overestimated by 50-100% due to the reflections. In regions where the temperature is in an intermediate range, say 175-200°C, underestimation due to the assumption of blackbody emission can be compensated by overestimation due to reflections, and it was estimated a 20% accuracy can be reached. In the edge Thomson scattering diagnostic, it was found that the reflected bremsstrahlung radiation from the divertor was minor compared with that from the core. On the other hand, in the wavelength range of < 800 nm, it was shown that the reflected line emission from the divertor can exceed the core bremsstrahlung, indicating that reflection can more than double the photon noise. Reflection of CXRS emission is sensitive to the ratio of diffuse to specular reflection $R_{\rm d}/R_{\rm s}$. The stray light level increases with the diffuse reflectivity, especially for $R_{\rm d}/R_{\rm s} < 20\%$. In a high density scenario, where the stray light level is high, the stray light can be up to $\sim$20% in the core when $R_{\rm d}/R_{\rm s}$ reaches $\sim 20\%$.

Considering the fact that the stray light level is significantly high for passive spectroscopy of the scrape off layer region, further studies investigating mitigation methodologies are of importance. E.g., for the optical dumps, it is of interest to optimize the shaping and position for each field of view. Characterization of the emission source, i.e. the emission profiles in divertor region, from divertor spectroscopic diagnostics with inclusion of reflection effects will be of importance. For infrared thermography, characterization of optical properties (emissivity and reflectivity) of the materials are of significant importance. Finally, for CXRS, the characterization of the optical properties including the ratio of specular to diffuse reflection is important to determine the influence of stray light. The detailed measurement of the bidirectional reflectance distribution function of different plasma facing materials is currently underway.

7. Acknowledgment

This work was supported in part by a Grant-in-Aid for Scientific Research (B) 15H04229 from the Japan Society for the Promotion of Science (JSPS).

The views and opinions expressed herein do not necessarily reflect those of the ITER Organization.

[1] E. M. Hollmann, A. Y. Pigarov and R. P. Doerner 2003 Review of Scientific Instruments **74** 3984.
[2] E. M. Hollmann and A. Y. Pigarov 2004 Contributions to Plasma Physics **44** 301.
[3] A. Kukushkin *et al.* 2013 EFDA-JET-CP(13)04/05 .
[4] B. Schunke, G. T. A. Huysmans and P. R. Thomas 2005 Review of Scientific Instruments **76** 083501.
[5] H. Meister, R. Dux, L. D. Horton, B. Kurzan, H. Zohm, the ASDEX Upgrade Team and P. J. McCarthy 2003 Review of Scientific Instruments **74** 4625.
[6] S. K. Rathgeber, R. Fischer, S. Fietz, J. Hobirk, A. Kallenbach, H. Meister, T. Putterich, F. Ryter, G. Tardini, E. Wolfrum and the ASDEX Upgrade Team 2010 Plasma Physics and Controlled Fusion **52** 095008.
[7] G. Verdoolaege, R. Fischer, G. V. Oost and J.-E. Contributors 2010 IEEE Transactions on Plasma Science **38** 3168.
[8] R. Reichle, J.-P. Lasserre, F. Oelhoffen, C. Desgranges, F. Faisse, L. Eupherte, C. Pocheau and M. Todeschini 2009 Physica Scripta **2009** 014029.
[9] M.-H. Aumeunier, M. Firdaouss, J.-M. Travère, T. Loarer, E. Gauthier, V. Martin, D. Chabaud, E. Humbert and J.-E. Contributors 2012 Rev. Sci. Instrum. **83** 10D522.
[10] M Kocan, R Reichle, M-H Aumeunier, J P Gunn, S Kajita, F Le Guern, S W Lisgo, T Loarer, A S Kukushkin, A Sashala Naik, F Rigollet, and B Stratton 2016 Phys. Scr. **T167** 014047.
[11] S. Kajita, E. Veshchev, S. Lisgo, R. Reichle, R. Barnsley, M. Walsh, A. Alekseev, A. Gorshkov, D. Vukolov, J. Stuber and S. Woodruff 2013 Plasma Physics and Controlled Fusion **55** 085020.
[12] S. Kajita, E. Veshchev, S. Lisgo, R. Barnsley, P. Morgan, M. Walsh, H. Ogawa, T. Sugie and K. Itami 2015 Journal of Nuclear Materials **463** 936 .
[13] A. B. Kukushkin, V. S. Neverov, A. G. Alekseev, S. W. Lisgo and A. S. Kukushkin 2016 Fusion Sci. Technol. **69** 628.
[14] S. Banerjee, P. Vasu, M. von Hellermann and R. J. E. Jaspers 2010 Plasma Physics and Controlled Fusion **52** 125006.
[15] S. Kajita, M. D. Bock, M. von Hellermann, A. Kukushkin and R. Barnsley 2015 Plasma Physics and Controlled Fusion **57** 045009.
[16] M.-H. Aumeunier and J.-M. Travere 2010 Review of Scientific Instruments **81** 10E524.
[17] M. Kocan, R. Pitts, S. Lisgo, A. Loarte, J. Gunn and V. Fuchs 2015 Journal of Nuclear Materials **463** 709 .
[18] LightTools web page. https://optics.synopsys.com/lighttools/ (Date of access: 06/06/2017).
[19] Zemax web page. http://www.zemax.com/ (Date of access: 06/06/2017).
[20] Optis web page. http://www.optis-world.com (Date of access: 24/08/2016).
[21] A. Kukushkin, H. Pacher, V. Kotov, G. Pacher and D. Reiter 2011 Fusion Engineering and Design **86** 2865 .
[22] S. Kajita, E. Veshchev, R. Barnsley and M. Walsh 2016 Contributions to Plasma Physics n/a.
[23] A. Kukushkin, V. Lisitsa, M. Kadomtsev, M. Levashova, V. Neverov, V. Shurygin, V. Kotov, A. Kukushkin, S. Lisgo, A. Alekseev, A. Gorshkov, D. Vukolov, K. Vukolov and E. Veshchev 2012 Proc. 24th IAEA Fusion Energy Conference, (San Diego, U.S.) ITR/P5.
[24] E. N. Andreenko, A. G. Alekseev, A. B. Kukushkin, V. S. Neverov, S. W. Lisgo and A. A. Morozov, Fusion Engineering and Design (in press).
[25] V. S. Neverov, A. Kukushkin, M. Stamp, A. Alekseev, S. Brezinsek and M. von Hellermann Nucl. Fusion **57** (2017) 016031.
[26] J. L. Terry, B. LaBombard, D. Brunner, J. Payne and G. A. Wurden 2010 Rev. Sci. Instrum. **81** 10E513.
[27] M. H. Aumeunier, J. M. Travere, R. Reichle, T. Loarer, E. Gauthier, D. Chabaud and E. Humbert 2012 IEEE Transactions on Plasma Science **40** 753.
[28] J. Bucalossi *et al.* 2011 Fusion Engineering and Design **86** 684 .
[29] E. Yatsuka, M. Bassan, T. Hatae, M. Ishikawa, T. Shimada, G. Vayakis, M. Walsh, R. Scannell, R. Huxford, P. Bilkova, P. Bohm, M. Aftanas and K. Itami 2013 Journal of Instrumentation **8**

C12001.

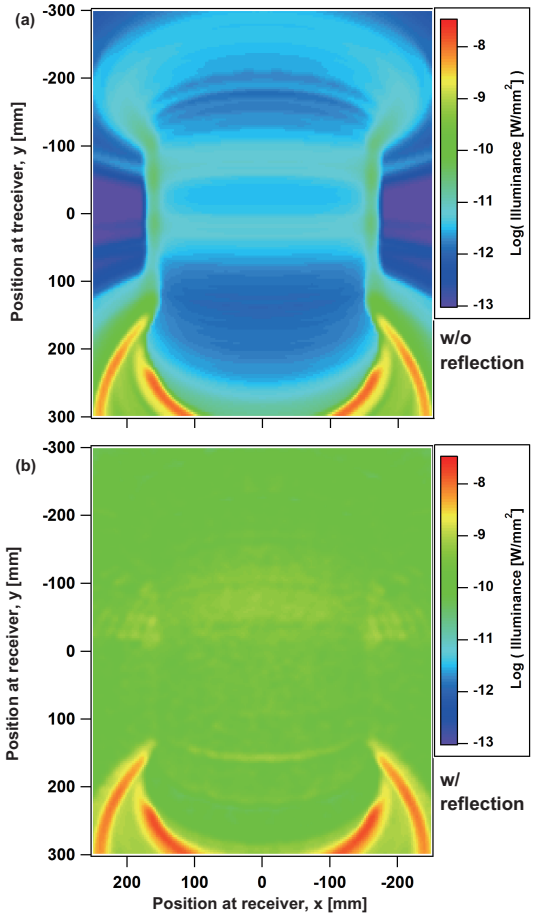

Figure 1. Simulated irradiance profiles of H_α using LightTools (a) without and (b) with wall reflection. The field of view corresponds to the one from the receiver B in Fig. 2.

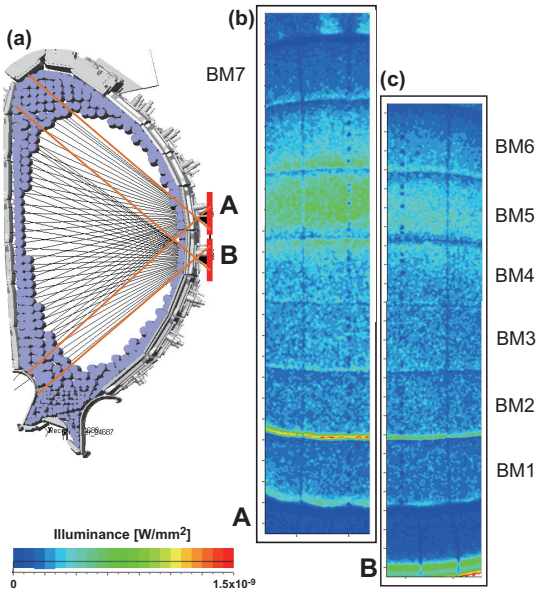

Figure 2. (a) Configuration of the simulation for detailed reflection profile from two different receivers, and reflection profiles observed from (b) the upper receiver A and (c) the lower receiver B on the equatorial port plug.

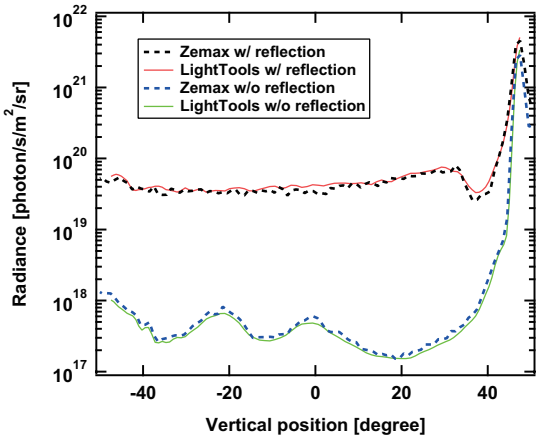

Figure 3. Comparison of simulations of the H-alpha signal in ITER with the Zemax and LightTools for the conditions of Fig. 1 for a smoothed first wall model. The radiance at a vertical line on the detector in the EPP11 is shown. The cases of no reflection from the wall and 50% reflectivity (49% diffuse and 1% specular) are considered.

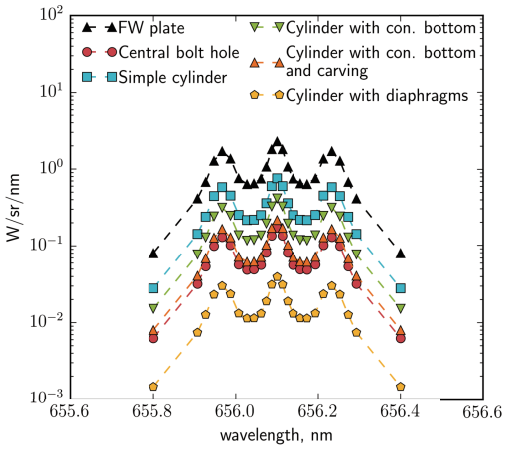

Figure 4. The calculated DSL spectra for the line of sight targeted at the first wall plate and at the five optical dumps of various design in the first wall of BM 4.

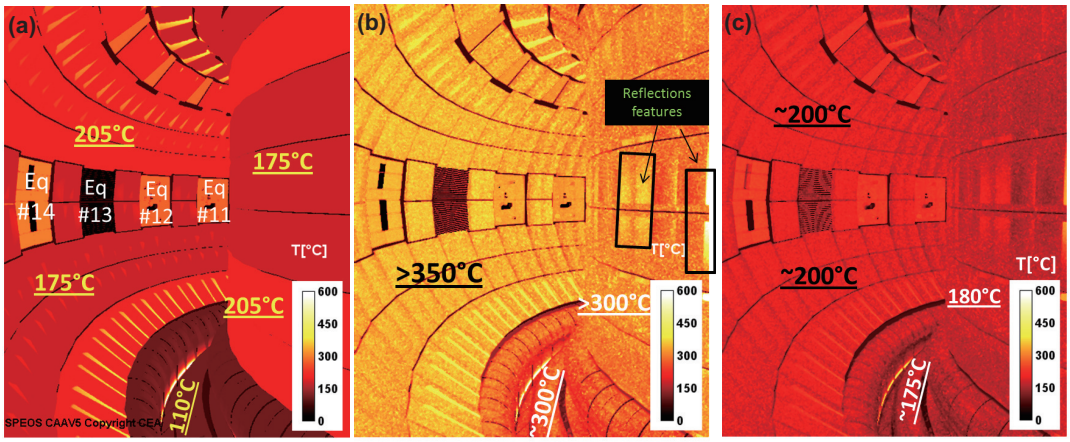

Figure 5. Infrared images as seen from the left tangential view of WAVS in equatorial port #17, simulated for the baseline burning plasma equilibrium: (a) true surface temperature map used as input for the photonic simulation, (b) equivalent gray body temperature maps (ϵ known and corrected) in a case of specular materials, and (c) equivalent blackbody temperature maps (ϵ=1) in a case of specular materials.

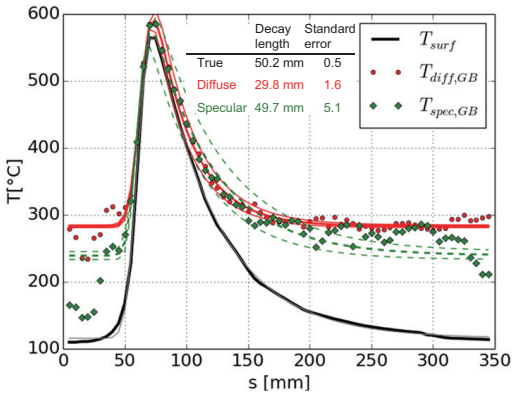

Figure 6. Predicted gray body (GB) Temperature profiles on inner vertical targets and their fits (solid and dashed lines) in the case of diffuse and specular materials. The exponential decay length is fitted from temperature profile.

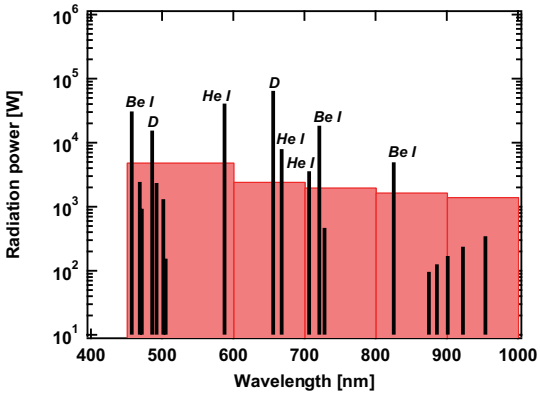

Figure 7. Comparison in the calculated radiation power between bremsstrahlung (rectangles) and line emissions (bars) spectra. Profiles of emissivity were calculated based on SOLPS4.3 modelling for the carbon-free ITER divertor case with Ne seeding, and the radiation power was summed up in the whole region modelled.

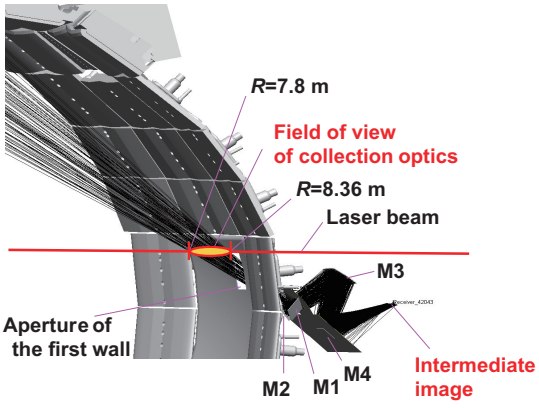

Figure 8. Model for evaluating intensity of background light on the edge Thomson scattering system.

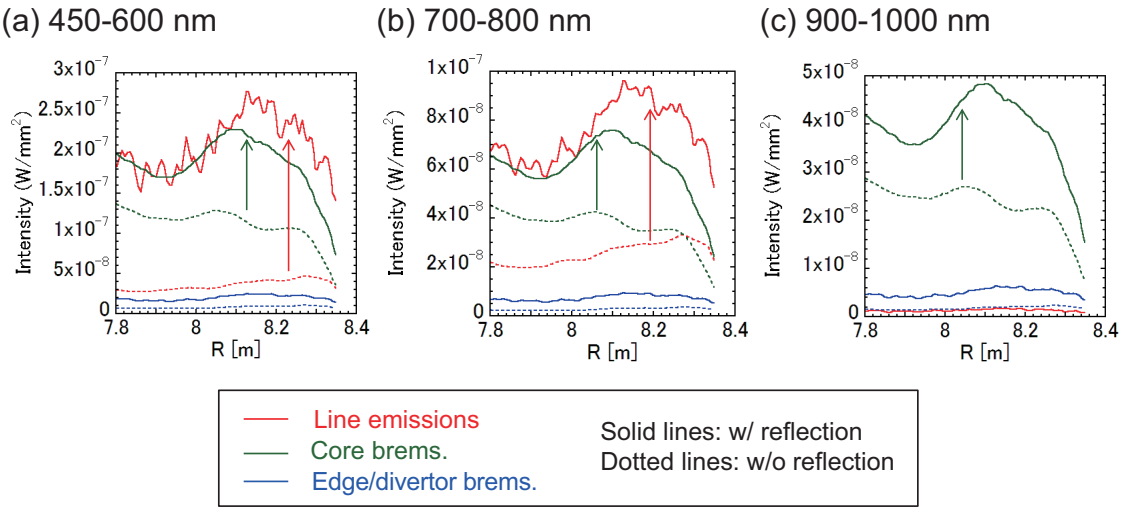

Figure 9. Expected intensity of background light on each line of sight within the wavelength ranges of (a) 450-600 nm, (b) 700-800 nm and (c) 900-1000 nm

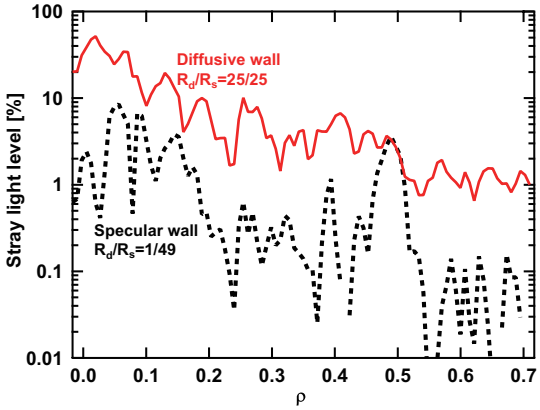

Figure 10. The stray light level as a function of ρ in a high density scenario. The ratios of diffuse to specular reflectivity, $R_{\rm d}/R_{\rm s}$, were assumed to be 1/49 and 25/25.

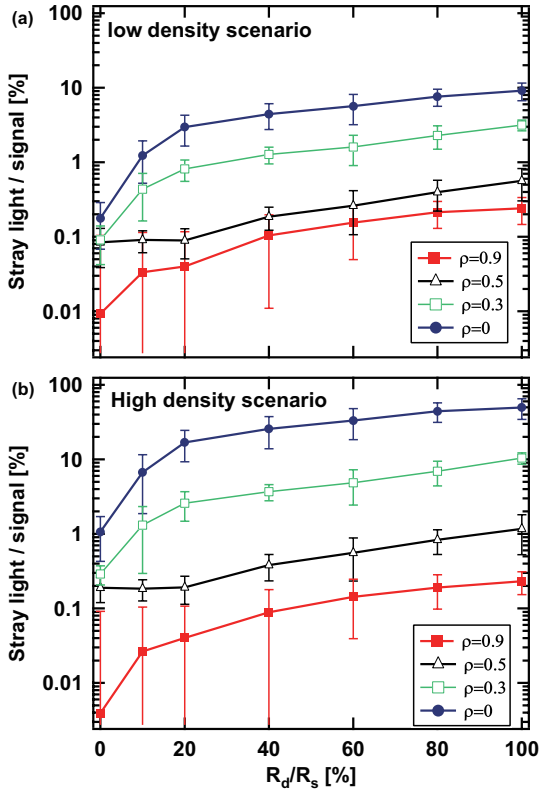

Figure 11. The ratio of the stray light to the signal in (a) low density and (a) high density scenarios as a function of $R_{\rm d}/R_{\rm s}$.